Performance of a concentrating photovoltaic monomodule under real operating conditions: Part I – Outdoor characterisation

Marios Theristis[1,*], Eduardo F. Fernández[2], George E. Georghiou[1], and Tadhg S. O'Donovan[3]

[1] PV Technology Laboratory, FOSS Research Centre for Sustainable Energy, Department of Electrical and Computer Engineering, University of Cyprus, Nicosia, 1678, Cyprus
[2] Centre for Advanced Studies in Energy and Environment (CEAEMA), IDEA Solar Energy Research Group, Electronics and Automation Engineering Department, University of Jaén, Las Lagunillas Campus, Jaén, 23071, Spain
[3] Institute of Mechanical, Process and Energy Engineering, Heriot-Watt University, Edinburgh, EH14 4AS, UK

* corresponding author email: theristis.marios@ucy.ac.cy

Abstract — Monitoring the performance of concentrating photovoltaic technologies under actual operating conditions is crucial for the prediction of energy yield. This requires an in-depth understanding of the behaviour of such systems through extensive outdoor characterisation and modelling. Detailed information on the outdoor performance of concentrating photovoltaic technology, taking into account the parameters that influence it, is therefore necessary for the evolution of the technology. In this work, a concentrating photovoltaic monomodule was characterised in a high desert climate (in Albuquerque, New Mexico). Due to the complexity of the outdoor performance evaluation of this technology, three relatively clear-sky days that exhibited different atmospheric conditions were selected in order to reduce the noise on the measured parameters and therefore provide a better understanding of its behaviour. One-minute resolution data were accumulated in order to assess the behaviour of the monomodule under real operating conditions. Initially, the monomodule is electrically characterised based on spectral changes. Different spectral indices are evaluated to enable a direct comparison amongst them. The diurnal electrical characteristics and temperature of the monomodule as a function of spectral, irradiance and ambient conditions is then analysed. The results of the three selected days show a maximum operating efficiency of 23.2% while maximum temperatures of 70.3°C and 67.6°C are observed on the diode and heat sink respectively. The importance of considering the influence of the atmospheric parameters on the performance of concentrating photovoltaics is also highlighted. In particular, spectral gains of up to 5% are exhibited due to lower aerosol content and higher precipitable water combined.

Keywords — concentrating photovoltaics, III-V multijunction solar cells, outdoor performance, solar spectrum, atmospheric parameters, real operating conditions

1. Introduction

Concentrating photovoltaics (CPV) using high-efficiency multijunction (MJ) solar cells have the potential to reduce costs at locations with high solar irradiance [1]. Such technologies are complex and inherently different than conventional photovoltaic (PV) technologies [2]. This is because, besides the tandem configuration of MJ solar cells that introduces a sensitivity to spectrum variations [3], they require an optical configuration to concentrate the direct sunlight and also an extended surface for heat dissipation [4].

Furthermore, even though CPV is a promising technology [5], it lacks detailed and high-quality field data, mainly because of the relatively young age of the technology [6]. As such, modelling the power output and characterising the technology under real operating conditions is important for identifying the parameters that affect system performance. This, in turn, can lead to further optimisation of the technology and improved energy yield prediction that is important for the market expansion of CPV [7]. A number of electrical models for the CPV energy yield prediction have been reported in the literature at the cell [8], module [9] and system [10] level with a varying degree of complexity and accuracy. However, understanding of the behaviour of such systems under different atmospheric conditions is paramount to increase its competitiveness. Although indoor testing of CPV [11] in laboratory (controlled) conditions can provide valuable information about their behaviour or optimisation, the real conditions in the field can vary significantly [12], due to variability in spectral irradiance, alignment or tracker errors, soiling, etc [13]. Therefore, the outdoor characterisation of CPV modules is important for performance assessment and power rating determination that could also lead to design improvements of the solar cell structure, concentrating optics, packaging or even of the requirements for cooling [14]. Moreover, it provides information about the sensitivity of the electrical parameters to the ambient, irradiance and spectral conditions. The spectrum varies with cloud cover and changing air mass (*AM*), aerosol optical depth (*AOD*) and precipitable water (*PW*) [15]. The understanding of the module's performance as a function of these parameters is significant in order to interpret any inconsistencies or anomalies in the measurements due to seasonal or even diurnal variation.

In this work, the outdoor performance of a CPV monomodule is presented in detail. Three relatively clear-sky days with different atmospheric conditions were selected in order to provide a better understanding of the monomodule’s behaviour and to also reduce the noise in the characterisation. The advantage of using a monomodule rather than a complete module is that electrical and optical mismatch losses along the series connected cells are neglected [16]. As such, the effect of the atmospheric parameters on the performance of the CPV technology can be extracted and evaluated. One-minute data capture resolution was used to evaluate the CPV monomodule’s performance, based on spectral variations. A detailed analysis follows on the electrical and thermal characteristics. The influence of the atmospheric parameters on the CPV performance is also discussed in detail including the comprehensive experimental analysis of the main spectral indices that are used in literature and the corresponding International Electrotechnical Commission (IEC) standards; to date, these have not been adequately compared. This, in particular, is useful for the better understanding of the relationship between the spectral indices which in turn, could be helpful for the selection of the appropriate index depending on the application or analysis [17]. Such detailed investigations are fundamental for the improvement of knowledge of the technology in order to achieve more accurate power ratings amongst different laboratories located around the world; this is the topic of Part II of this work [18].

2. Spectral indices

According to the IEC 62670-3 [19], the spectral conditions are monitored using the spectral matching ratio (*SMR*) as a criterion. *SMR* between two subcells is defined as the ratio of the measured short-circuit current density of one subcell at a specific spectrum to the short-circuit current density at reference conditions (i.e. the ASTM G173-03 AM1.5D spectrum [20]) divided by the same ratio of the other subcell. In the case of triple-junction (3J) solar cells, *SMR1* of top to middle subcell is described as [21]:

$$SMR1 = \frac{J_{sc}^{top}}{J_{sc,ref}^{top}} \Big/ \frac{J_{sc}^{mid}}{J_{sc,ref}^{mid}} \quad \textbf{(1)}$$

where the short-circuit current of *i* subcell (J_{sc}^{i}) is calculated as:

$$J_{sc}^{i} = \int SR_i(\lambda) \cdot DNI(\lambda) \cdot \eta_{opt}(\lambda) d\lambda \quad \textbf{(2)}$$

where *DNI* is the direct normal irradiance, η_{opt} is the optical efficiency, *SR* is the spectral response (i.e. the ratio of current generation to the incident power) and λ is the wavelength. The subscript, "*ref*", denotes the reference conditions. Due to the corresponding absorption bands of the top and middle subcells, *SMR1* > 1 refers to a blue-rich incident spectrum (i.e. higher effective irradiance on the top junction) and *SMR1* < 1 refers to a red-rich incident spectrum (i.e. higher effective irradiance on the middle junction). The *SMR1* = 1 when the incident spectrum matches the reference conditions. In a similar manner, the *SMR2* of middle to bottom subcell becomes:

$$SMR2 = \frac{J_{sc}^{mid}}{J_{sc,ref}^{mid}} \bigg/ \frac{J_{sc}^{bot}}{J_{sc,ref}^{bot}} \quad (3)$$

Unlike the *SMR1*, *SMR2* (i.e. middle to bottom) is not described quantitatively in literature, but in general term: the higher the value of *SMR2*, the higher the *PW* is (i.e. wetter atmosphere) [22]. This is attributed to the large attenuation of *PW* in the near-infrared region of the spectrum which is where the spectral absorption of the bottom subcell corresponds [23]. An additional *SMR* index, i.e. top to bottom subcell, *SMR3*, can also be defined within a 3J solar cell, however, *SMR3* is "redundant" and usually neglected [24].

Another important spectral index that is not mentioned in IEC 62670-3, but is used in this study for the outdoor characterisation, is the spectral mismatch factor defined in IEC 60904-7 [25] (often referred to as spectral factor, *SF*) [26] which is basically a normalisation of the J_{sc}. This index allows the quantification of the spectral performance (spectral gains or losses) of a particular device, compared to the reference spectrum AM1.5. In the case of multijunction solar cells, the *SF* of each subcell is given by [27]:

$$SF_i = \frac{J_{sc}^{i}}{DNI} \cdot \frac{DNI_{ref}}{J_{sc,ref}^{i}} \quad (4)$$

The output current of a 3J solar cell is restricted to the minimum current of the three subcells because of the in-series connection. Therefore, the *SF* of the whole device is given by:

$$SF = \frac{\min(J_{sc}^{i})}{DNI} \cdot \frac{DNI_{ref}}{\min(J_{sc,ref}^{i})} \quad (5)$$

where the subscript "*i*" denotes the corresponding subcell. *SF* values above 1 indicate spectral gains, below 1 indicate spectral losses and equal to 1 indicates the same spectral conditions as the reference (i.e. AM1.5D). In cases where a spectroradiometer device is not available, the *SF* can be estimated using the reference and measured short-circuit currents and direct normal irradiances.

Both of these spectral indices (*SF* and *SMR*) have been widely used in the PV community [17]. It is worth mentioning that because the 3J solar cells are monolothically connected (i.e. no access to individual subcell), the SF_i and *SMR* indices can be either evaluated by using component cells (also called isotypes) or by calculating the corresponding spectral index under the prevailing spectrum [28]. Component cells have the same composition as 3J III-V solar cells but with only one active p-n junction [29] and can therefore allow the characterisation at the subcell level.

3. Experimental setup

In order to conduct this study, a CPV monomodule (Suncore DDM-1090×) was installed at the outdoor test facility of CFV solar test laboratory in Albuquerque, New Mexico (NM). The DDM-1090× consists of a silicon-on-glass (SoG) Fresnel lens as the primary concentrator optic and an EMCORE 10 x 10 mm triple-junction solar cell bonded to a direct bonded copper (DBC) substrate. A refractive truncated pyramid is attached on the solar cell as a homogeniser. The DBC substrate is placed on an aluminium finned heat sink for heat dissipation. The rated power of the EMCORE solar cell is 17.50 W at an irradiance intensity of 50 W/cm^2 and the geometric concentration ratio of the monomodule is 1090× with an acceptance angle of approximately ±0.7°. The monomodule's detailed geometry is described in our previous work [16]. Photographs of the receiver and monomodule are illustrated in Figure 1.

Figure 1: A CPV receiver assembly using an EMCORE solar cell bonded on a DBC and an aluminium heat sink (left) and a photograph of two DDM-1090× monomodules mounted on the solar tracker in Albuquerque, NM (right).

The monomodule was mounted on a high accuracy (within 0.3°) two-axis solar tracker. The meteorological conditions were monitored through a Vaisala weather transmitter WXT520 while the irradiance was measured using a CHP1 pyrheliometer (*DNI*) and a CMP6 pyranometer (global normal, *GNI*). The spectral conditions (and *SMR* indices in particular) were evaluated according to IEC 62670-3 using a set of Black Photon Instruments (BPI) isotype sensors and the atmospheric parameters that affect the spectral composition (i.e. *AOD* and *PW*) were measured using a Solar Light Microtops II sunphotometer. It should be noted that isotype sensors do not incorporate any concentrating optics and therefore, the η_{opt} in Eq. (2) is equal to unity in this case. For the estimation of *SF*, the measured and reference short-circuit currents and direct normal irradiances were used, as mentioned in Section 2. The reference short-circuit current was measured using a Helios 3198 solar simulator; the details of the experimental setup are discussed in Part II of this work. The tracker's accuracy was monitored using a BPI tracking accuracy sensor. Finally, the current-voltage (*I-V*) characteristics of the monomodule were traced using a Daystar DS-1000 *I-V* curve tracer. A T-type thermocouple (TC) was embedded onto the diode package within the receiver and an additional TC was placed in the centre of the heat sink's base. A list of equipment and the associated accuracies are given in Table 1. The meteorological, irradiance, spectral and temperature measurements were recorded in the SQL database once every minute using a Campbell Scientific CR1000 datalogger. The *I-V* measurements were logged on a laptop every minute also and then transferred to the database. The monomodule's alignment was checked periodically and it was cleaned at least once a week or after rain. The installed sensors were within the calibration period and frequent inspections were performed to ensure good quality measurements.

Equipment	Measurement	Accuracy
Kipp & Zonen CHP1	Direct normal irradiance	±1%
Kipp & Zonen CMP6	Global normal irradiance	±5%
BPI top cell	Irradiance 375 – 700 nm	±2.5%
BPI middle cell	Irradiance 700 – 900 nm	±2.5%
BPI bottom cell	Irradiance 900 – 1750 nm	±5%
BPI tracking accuracy sensor	Azimuth and elevation pointing errors	0.028°
Daystar DS-1000	Voltage	±0.15%
Daystar DS-1000	Current	±0.1%
Calculation	Power	±0.18%
Solar Light Microtops II	Atmospheric parameters	±2%
T-type thermocouple	Heat sink and diode temperatures	±1°C
Vaisala WXT520 anemometer	Wind speed	< 3%
Vaisala WXT520 thermometer	Ambient temperature	< 0.7°C

Table 1: Accuracy of measuring equipment.

4. Performance of CPV monomodule

The frequency distribution of the irradiance and ambient conditions from 25/06/2015 to 21/08/2015 in Albuquerque, NM are shown in Figures 2, 3, 4 for *DNI*, ambient temperature (T_{amb}) and wind speed (*WS*) respectively. The distribution of *AM* is also given in Figure 5. It has to be noted that these figures contain raw data (i.e. no filtering) and that during rainy and cloudy instances or days, no measurements were taken.

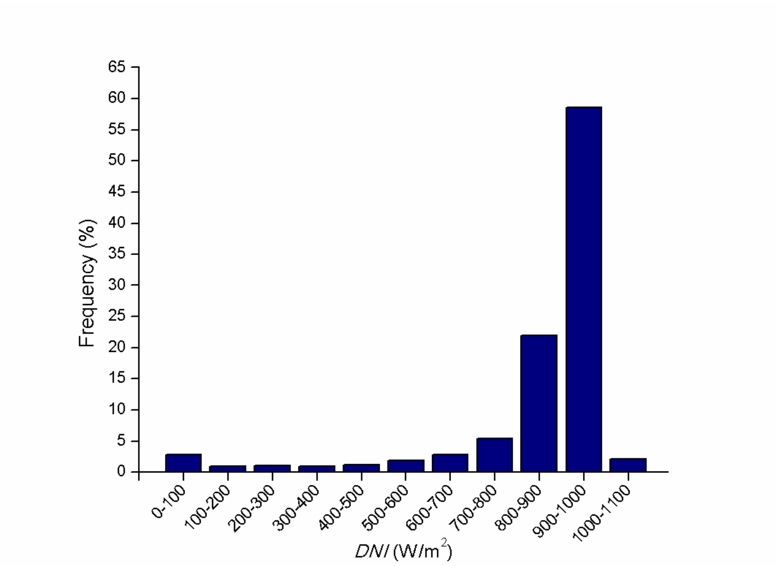

Figure 2: *DNI* distribution over the period that the experiments were conducted in Albuquerque, NM.

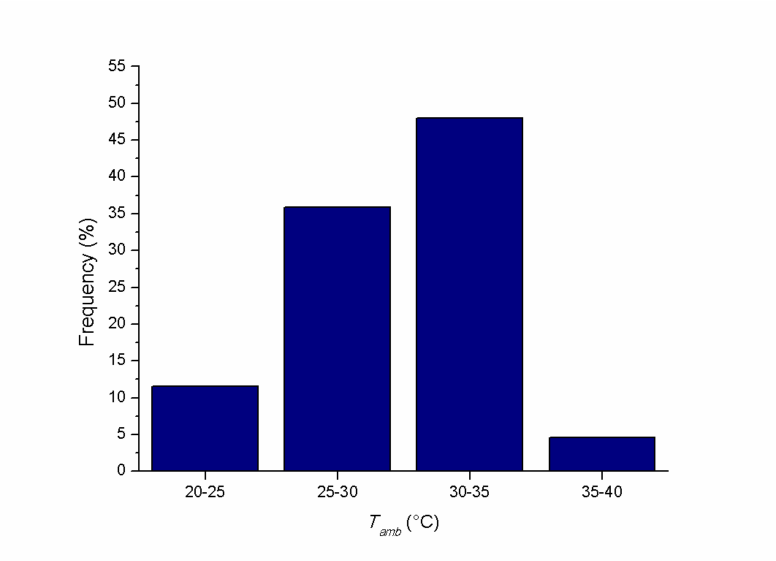

Figure 3: T_{amb} distribution over the period that the experiments were conducted in Albuquerque, NM.

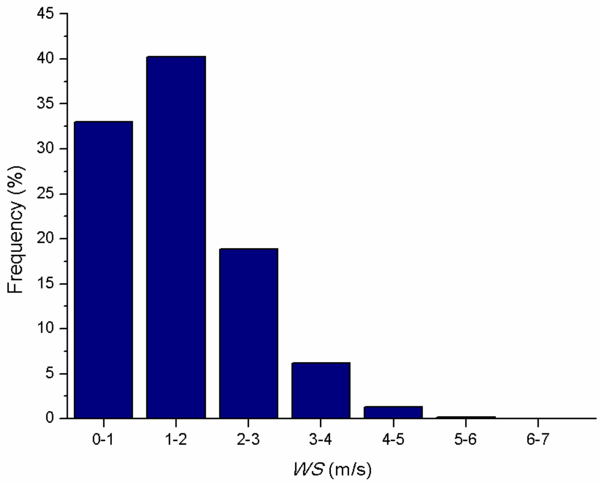

Figure 4: ***WS*** **distribution over the period that the experiments were conducted in Albuquerque, NM.**

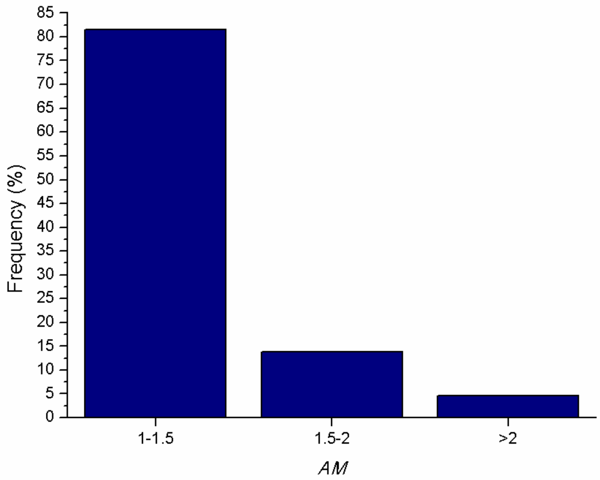

Figure 5: ***AM*** **distribution over the period that the experiments were conducted in Albuquerque, NM.**

New Mexico is affected by the North American Monsoon System every Summer [30] and therefore during the measurement periods, most mornings were characterised by a relatively clear-sky, while most of the afternoons were characterised by heavy clouds and rain and/or thunderstorms. In order to capture the effects of spectrum changes over a course of a day, only three relatively clear-sky days with different atmospheric parameters occurred and therefore were selected for the evaluation of the outdoor testing; these days were: 03/08/2015, 13/08/2015 and 19/08/2015. The selection of only three days with different atmospheric parameters enabled the noise removal that typically occurs on outdoor characterisation data of CPV systems. As such, the dependence of the CPV monomodule against the atmospheric parameters could be captured and analysed. The data were filtered for 1-minute *DNI* variation < 2%; this resulted in 1735 datapoints out of 1781 (raw datapoints), i.e. 614, 600, 521 datapoints for 03/08/2015, 13/08/2015 and 19/08/2015 respectively.

4.1. Spectral performance

As mentioned earlier, the spectral and broadband (i.e. integrated over all wavelengths) solar irradiance in Earth's surface is affected by a number of factors such as the changes in *AM* and atmospheric effects. The *AM* is defined as the "path length through the atmosphere relative to the zenith (overhead position) [31]" and taking into account the curvature of Earth, it is calculated by [32]:

$$AM = \frac{1}{\cos(z) + 0.50572(96.07995 - z)^{-1.6364}} \tag{6}$$

where *z* is the zenith angle and is defined as the angle between the sun's position and the zenith.

Figure 6 shows the *AM* diurnal variation during the three selected days; an increase in *AM* can be noticed with each passing day since the measurements were taken after the Summer solstice. The sunphotometer measurements are given in Figures 7 and 8 for *AOD* and *PW* respectively. The maximum *AOD* change during a single day was 0.02, 0.05, 0.09 on 03/08/2015, 13/08/2015, 19/08/2015 respectively. Similarly, the maximum *PW* change during a single day was 0.75 cm, 0.23 cm, 0.26 cm on 03/08/2015, 13/08/2015, 19/08/2015 respectively. The average values are given in Table 2. It can be seen that on 03/08/2015 the lowest average *AOD* and highest average *PW* occurred while on the 19/08/2015 the highest *AOD* and lowest *PW* occurred.

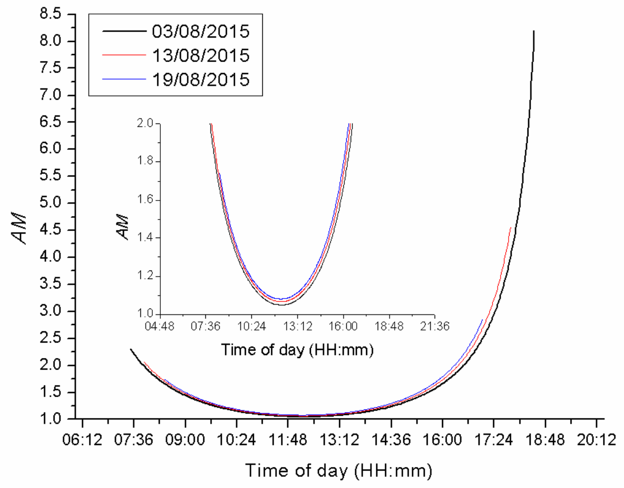

Figure 6: ***AM*** **variation over a course of the day on the 03/08/2015, 13/08/2015, 19/08/2015 in Albuquerque, NM.**

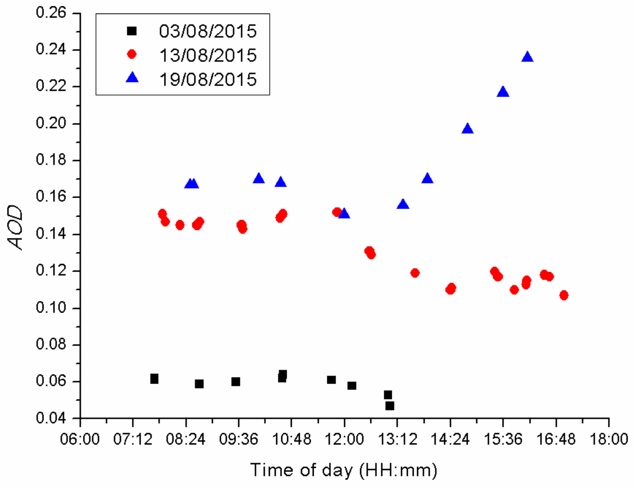

Figure 7: ***AOD*** **variation over a course of the day on the 03/08/2015, 13/08/2015, 19/08/2015 in Albuquerque, NM.**

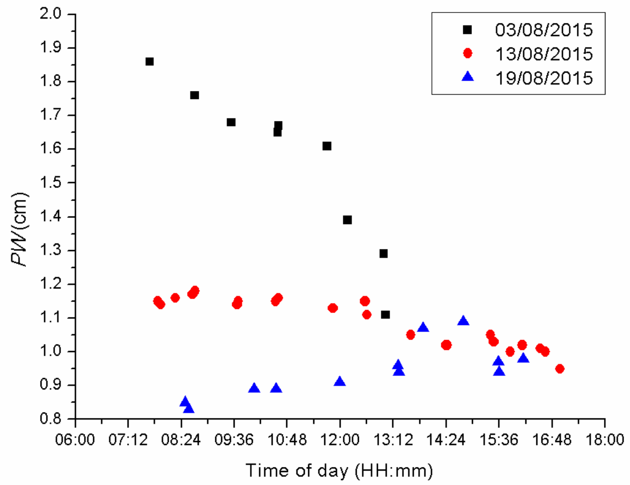

Figure 8: *PW* variation over a course of the day on the 03/08/2015, 13/08/2015, 19/08/2015 in Albuquerque, NM.

Date	*AOD*	*PW* (cm)
03/08/2015	0.06	1.59
13/08/2015	0.13	1.09
19/08/2015	0.18	0.94

Table 2: Average daily values of *AOD* and *PW* for 3rd, 13th, 19th of August 2015 in Albuquerque, NM.

The diurnal *DNI* variation is shown in Figure 9; since the *DNI* is affected by *AM* and *AOD* to a higher degree than *PW* [33], it can be seen that the *DNI* is higher on the 03/08/2015 because of the lower *AM* and *AOD* values. In addition, on the 13/08/2015 and the 19/08/2015 the diurnal variation of *DNI* is similar until around noon, where the *AOD* values are also similar (see Figure 7), and that during the afternoon the *DNI* is lower on the 19/08/2015 because of the increase in *AOD*.

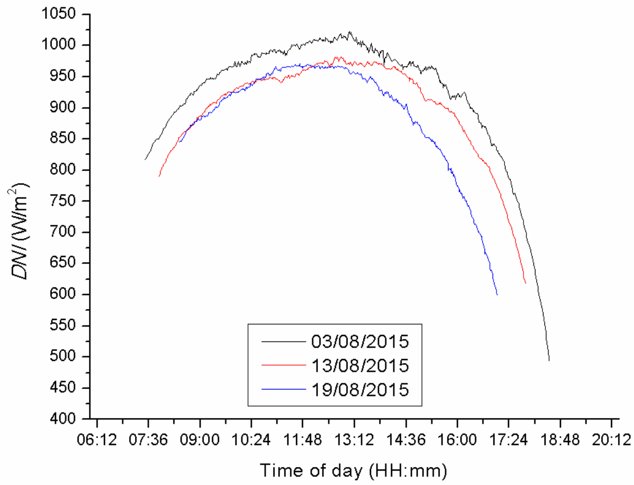

Figure 9: Diurnal variation of *DNI* on the 03/08/2015, 13/08/2015, 19/08/2015 in Albuquerque, NM.

The *DNI* decreases with increasing *AM* as expected and as illustrated in Figure 10. However, the *AM* influence on *DNI* during the morning hours is different than the afternoon hours and that is mainly due to the *AOD* content in the atmosphere. While on the 03/08/2015 and the 13/08/2015, the *DNI* is lower during the morning hours; on the 19/08/2015 the trend is different, exhibiting higher *DNI* during the morning as compared to the *DNI* measured in the afternoon. This can be explained, again, by comparing Figures 7, 9 and 10 where it can be seen that on the 03/08/2015 (although not enough data, the trend can be assumed to decrease around noon) and the 13/08/2015 the *AOD* is reduced in the afternoon while on the 19/08/2015 the *AOD* is increased.

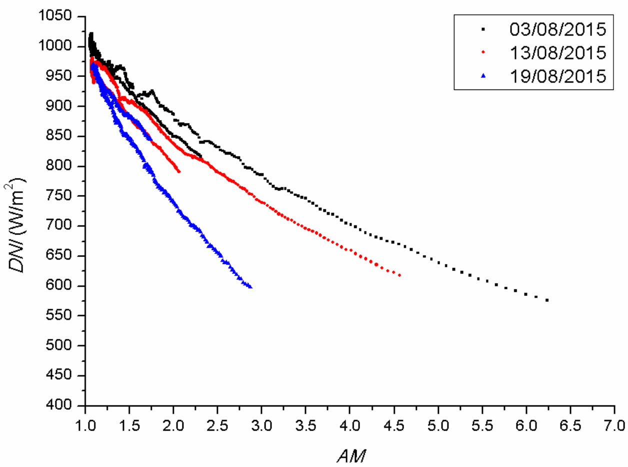

Figure 10: DNI as a function of *AM* on the 03/08/2015, 13/08/2015, 19/08/2015 in Albuquerque, NM.

The *SF* variation as a function of *AM* is shown in Figure 11. On the 03/08/2015, the diurnal variation of *SF* is roughly divided into three areas: morning, afternoon, sunset (see also Figure 12). In the morning hours, for *AM* < 2.5, the *SF* ≈ 1.05 at 7:37 am (*AM* = 2.3, *AOD* ≈ 0.06 and *PW* ≈ 1.9 cm) and decreases below *SF* = 1 at around 10 am (*AM* < 1.25, *AOD* ≈ 0.06 and *PW* ≈ 1.65 cm) down to *SF* = 0.98 at around 12:15 pm (*AM* ≈ 1.05, *AOD* ≈ 0.06 and *PW* ≈ 1.4 cm). During the afternoon, the *SF* slowly increases with increasing *AM* up to *SF* ≈ 1.03 at around 17:30 pm (*AM* ≈ 3.2, no atmospheric data available) where it decreases again almost linearly (for approximately *AM* > 4) during the rapid increase of *AM* (i.e. sunset). The lower peak in Figure 12 between morning and afternoon hours can be explained by the decrease of the *PW* during the day (see Figure 8). Similar behaviours, but to a lesser extent, are noticed on the 13/08/2015 and 19/08/2015; this is mainly due to the higher *AOD* and lower *PW* during those days (see Table 2). By comparing these two days, it can be seen that spectral gains (i.e. *SF* > 1) occurred only during the morning of the 13/08/2015 (until 8:20 am approximately). On the 19/08/2015, the *SF* < 1 during the day, due to the lower *PW* and the increased *AOD* after around noon (see Figure 7); this can explain the "collapse" in Figures 11 and 12. In addition, the arrow in Figure 11 indicates the decreasing *AOD* and increasing *PW* similar to results presented by Muller *et al*. [34], where the I_{sc}/DNI (where I_{sc} is the short-circuit current) change was used as a criterion. More details explaining the behaviour can be found in [33].

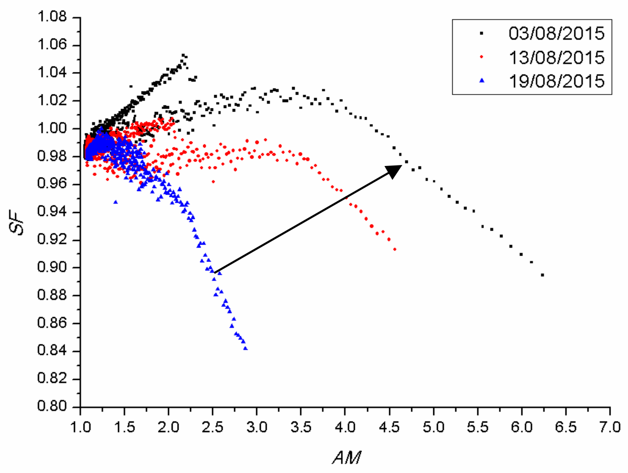

Figure 11: *SF* as a function of *AM* on the 03/08/2015, 13/08/2015, 19/08/2015 in Albuquerque, NM. The arrow indicates decreasing *AOD* and increasing *PW*.

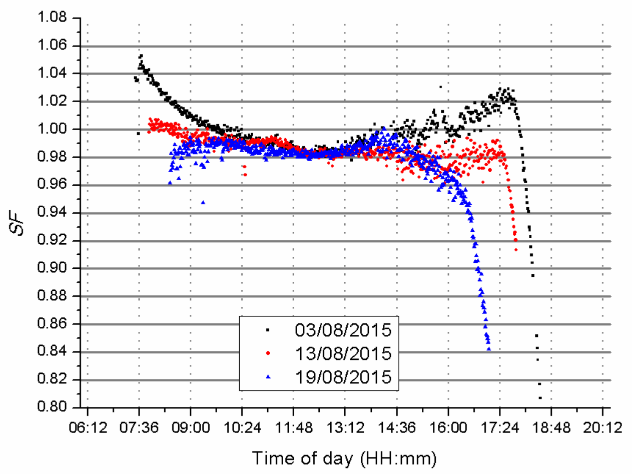

Figure 12: Diurnal variation of *SF* on the 03/08/2015, 13/08/2015, 19/08/2015 in Albuquerque, NM.

As mentioned in Section 3, BPI isotype (or component) cells were used to characterise the spectral solar irradiance. Such devices have the same composition as 3J III-V solar cells but with only one active p-n junction [29]. Therefore, they can provide information about the current generation at each subcell of a 3J III-V solar cell which in turn can be used to characterise the spectrum through the *SMR* index, described in Section 2.

SMR1 and *SMR2* were plotted against *AM* in Figures 13 and 14 respectively. Similar to the earlier discussion, the *SMR* indices on the 03/08/2015 are also higher compared to the other days in both cases (*SMR1* and *SMR2*) due to the lower *AOD* and higher *PW*. The *SMR1* on the 03/08/2015 is slightly higher (by up to ~ 0.002) in the morning due to the higher (compared to the afternoon) *PW*; similarly *SMR2* during the morning of the same day is higher (by up to ~ 0.05). On the 13/08/2015 however, the *SMR1* starts lower (= 0.94) and increases during the afternoon for *AM* < 2, due to the reduction in *AOD*. In Figure 15, the diurnal variations of *SMR1* and *SMR2* are shown; overall, it is obvious that the highest *SMR1* and *SMR2* occur during the 03/08/2015 due to the lowest *AOD* and highest *PW*. Also, similar to the *SF*, it can be seen that the *SMR2* during the afternoon (see also Figure 13) is lower than at the beginning of the day because of the *PW* reduction. The same effects as in Figure 9 can be seen on the 13/08/2015 and the 19/08/2015; after around 12 pm the *SMR1* is higher on the 13/08/2015 than on the 19/08/2015, because of the increase in *AOD* on the 19/08/2015. A sudden drop was observed in *SMR2* similar to *SF* (Figure 12) due to the increase in *AOD* after noon of the 19/08/2015. In addition, the spectrum can be considered blue rich for the largest part of the day.

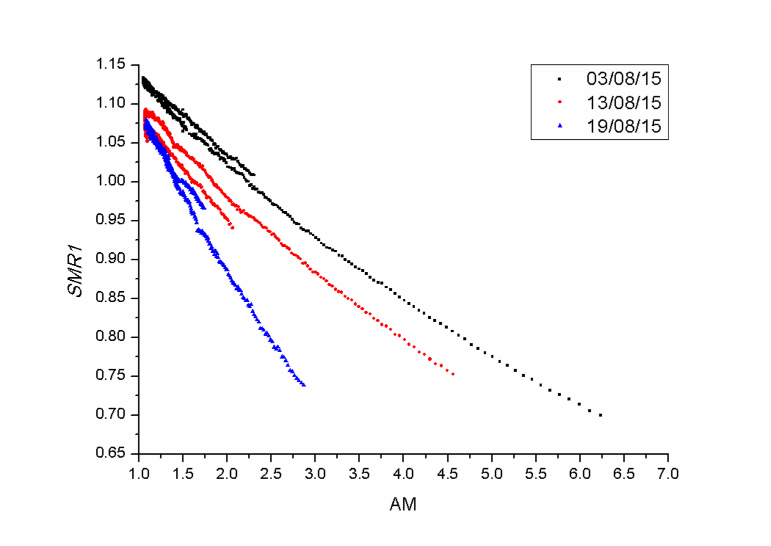

Figure 13: *SMR1* as a function of *AM* on the 03/08/2015, 13/08/2015, 19/08/2015 in Albuquerque, NM.

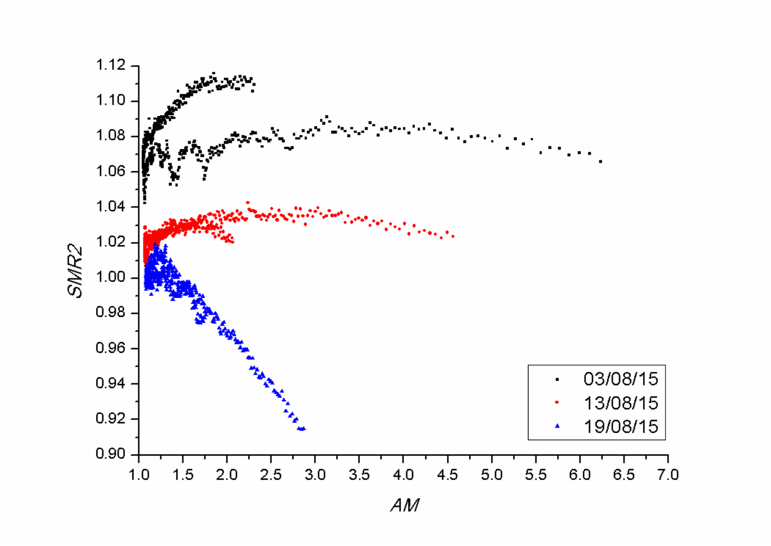

Figure 14: *SMR2* as a function of *AM* on the 03/08/2015, 13/08/2015, 19/08/2015 in Albuquerque, NM

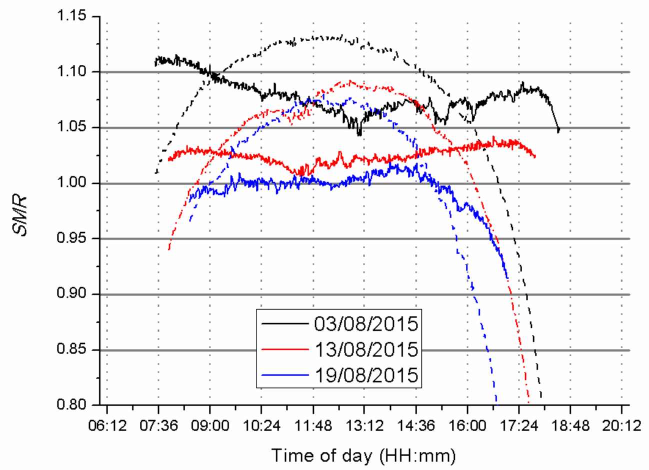

Figure 15: Diurnal variation of *SMR1* (dash lines) and *SMR2* (solid lines) on the 03/08/2015 (black colour), 13/08/2015 (red colour), 19/08/2015 (blue colour) in Albuquerque, NM. (For a better interpretation of this plot, the reader is referred to the web version of this article.)

The relationship between *SMR1* and *SF* is shown in Figure 16. Overall, the trend is similar to the modelled data published in [35]; the *SF* increases with increasing *SMR1* until it reaches the maximum and then it decreases. On the 03/08/2015, the *SF* presents gains of up to 5% for the majority of the day while the spectrum is blue-rich. On the 13/08/2015 spectral gains of up to 1% occur while the spectrum is on the "boundary" between blue- and red-rich; on the 19/08/2015 no spectral gains occur even when the solar spectrum is blue-rich.

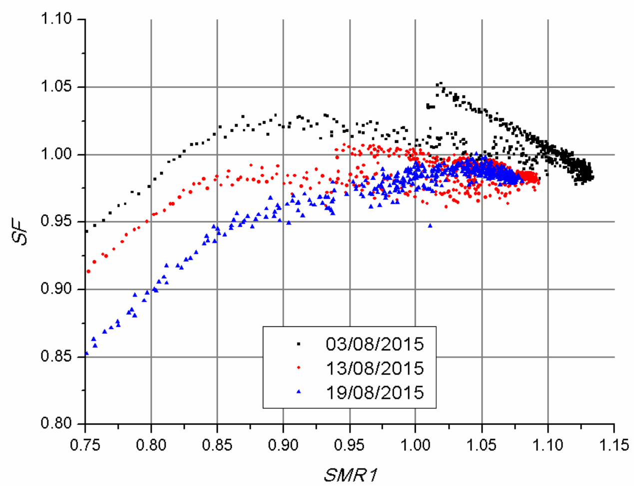

Figure 16: *SF* as a function of *SMR1* on the 03/08/2015, 13/08/2015, 19/08/2015 in Albuquerque, NM.

4.2. Electrical and thermal performance

The irradiance and ambient conditions (*DNI*, *DNI*/*GNI* ratio, T_{amb} and *WS*) during the selected days are shown in Figure 17. For comparison purposes the *DNI* figure is repeated; on the 03/08/2015, the highest *DNI* was measured at 1022 W/m^2 mainly due to the lowest *AOD* and *PW*, as explained earlier. The *DNI*/*GNI* ratio shows that on the 03/08/2015, some "light haziness in the sky" introduced some spikes, although the ratio was still above 0.8 (i.e. less than 20% diffuse irradiance). The highest T_{amb} was 34.8°C and was recorded on the 13/08/2015 while the minimum was 21.2°C during the early morning of the 03/08/2015. The *WS* on the 03/08/2015 and the 13/08/2015 was similar, while on the 19/08/2015 the morning was windy with a maximum *WS* of 6.5 m/s.

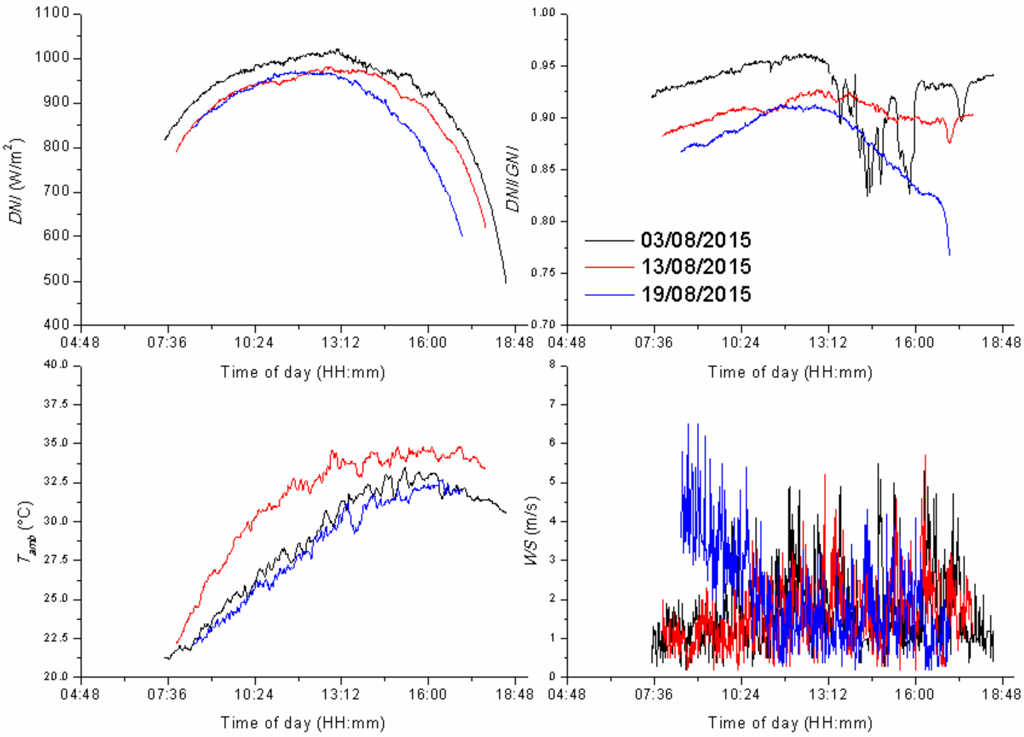

Figure 17: Diurnal variation of *DNI* (top left), *DNI*/*GNI* ratio (top right), T_{amb} (bottom left) and *WS* (bottom right) on the 03/08/2015, 13/08/2015, 19/08/2015 in Albuquerque, NM. The top left *DNI* figure is repeated for comparison purposes.

Figure 18 shows the diurnal variation of measured electrical parameters: maximum power, short-circuit current, open-circuit voltage and fill factor (P_{mp}, I_{sc}, V_{oc} and *FF* respectively). As expected, since *DNI* is the dominant parameter that affects the electrical performance, the I_{sc} and hence the P_{mp} follows the same trend as the *DNI*. The maximum P_{mp}, I_{sc}, V_{oc} and *FF* were 23.1 W, 11.58 A, 2.98 V and 83% respectively. It can be observed that *FF* exhibits similar behaviour to *AM* which is the dominant parameter that affects the spectrum. This can be explained by the fact that *FF* tends to decrease with increasing spectral performance of MJ-based CPV devices, as previoulsly reported by McMahon *et al*. [36] and Fernández *et al*. [37]. Despite this, the temperature effects also play an important role. Indeed, V_{oc} and *FF* exhibit their lowest values during midday to afternoon due to the higher temperatures. During the morning of the 19/08/2015 the V_{oc} and *FF* is higher due to the higher *WS* and lower T_{amb}.

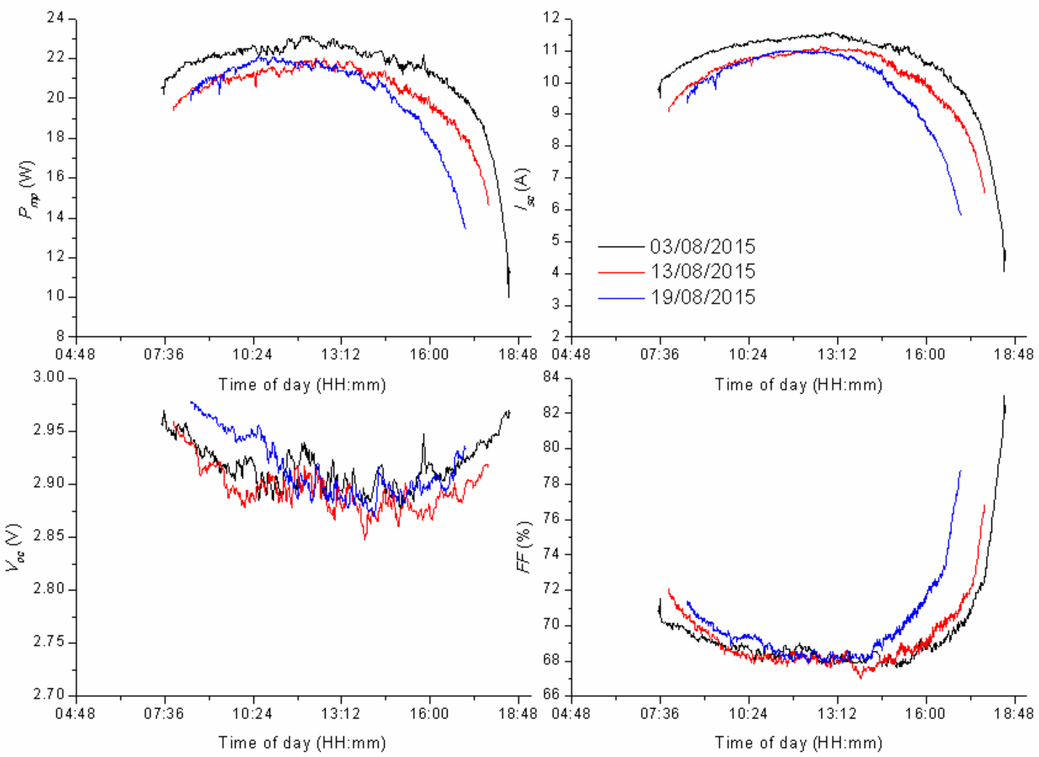

Figure 18: Diurnal variation of P_{mp} (top left), I_{sc} (top right), V_{oc} (bottom left) and *FF* (bottom right) on the 03/08/2015, 13/08/2015, 19/08/2015 in Albuquerque, NM.

In addition, the diode and heat sink temperatures (T_{diode} and T_{HS} respectively) are illustrated in Figure 19; the highest average temperatures were measured on the 13/08/2015 with T_{diode} = 61.7°C and T_{HS} = 57.4°C; this can be attributed to the T_{amb}, because although the *DNI* is lower (compared to the 03/08/2015), the T_{amb} is higher (by an average of 3°C) and therefore contributes to the higher temperatures. On the same day the maximum T_{diode} = 70.3°C and T_{HS} = 67.6°C. Minimum, maximum and average T_{diode} and T_{HS} are given in Tables 3 and 4 respectively.

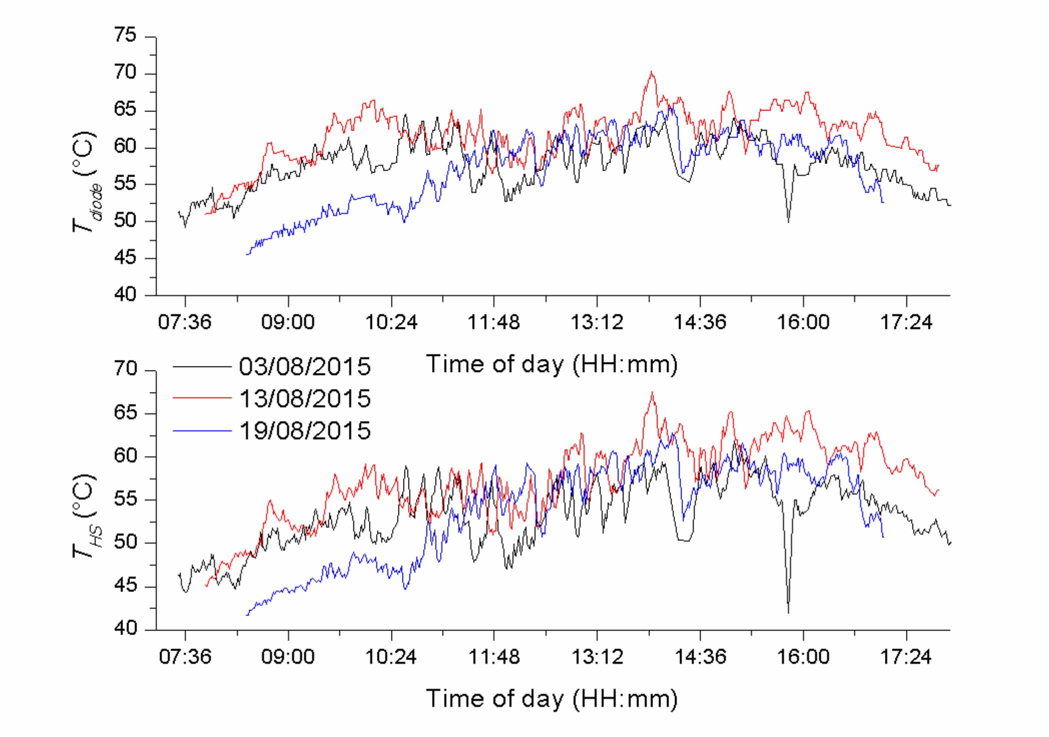

Figure 19: Diurnal variation of T_{diode} (top figure) and T_{HS} (bottom figure) on the 03/08/2015, 13/08/2015, 19/08/2015 in Albuquerque, NM.

T_{diode} (°C)	Minimum	Maximum	Average
03/08/2015	46.00	64.49	57.35
13/08/2015	51.04	70.32	61.71
19/08/2015	45.63	65.50	57.27

Table 3: Minimum, maximum and average T_{diode} measured on the 03/08/2015, 13/08/2015, 19/08/2015 in Albuquerque, NM.

T_{HS} (°C)	Minimum	Maximum	Average
03/08/2015	41.97	61.88	53.01
13/08/2015	45.05	67.56	57.36
19/08/2015	41.70	62.78	53.81

Table 4: Minimum, maximum and average T_{HS} measured on the 03/08/2015, 13/08/2015, 19/08/2015 in Albuquerque, NM.

The linear relationship between I_{sc} and *DNI* is shown in Figure 20 for all three days for a *DNI* between approximately 500 W/m^2 and approximately 1050 W/m^2. The coefficients of determination (R^2) of the linear fits for each day and all together are given in Table 5 and it ranges between 0.967 to 0.992. Although Figure 20 shows that the I_{sc} is predominantly affected linearly by the *DNI* as a first approximation [6], it is also important to evaluate the spectral sensitivity of MJ solar cells [34]. This can also be verified by noting the change in the slope of I_{sc} at approximately 700 W/m^2 for the three days considered. Indeed, by considering Figures 15 and 17 (top left), it can be seen that *SMR1* equals unity at approximately that irradiance level. Hence, the variation in the slope can be attributed to the change of the limiting subcell, i.e. the middle subcell is limiting at *SMR1* > 1 while the top subcell at *SMR1* < 1.

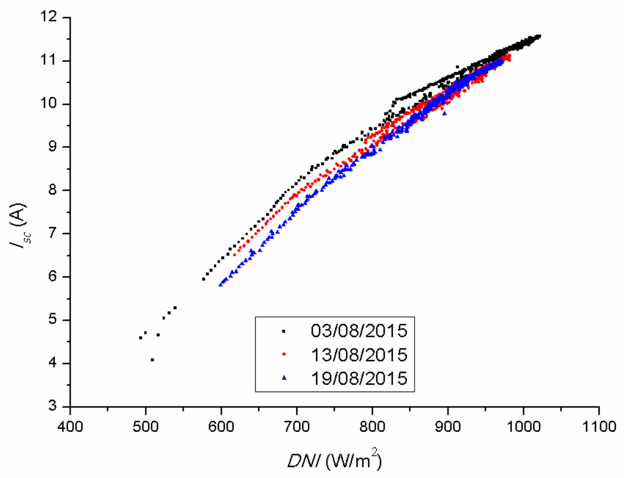

Figure 20: I_{sc} as a function of *DNI* on the 03/08/2015, 13/08/2015, 19/08/2015 in Albuquerque, NM.

Day	03/08/2015	13/08/2015	19/08/2015	All
R^2	0.967	0.989	0.992	0.974

Table 5: R^2 values obtained by linear fit of I_{sc} Vs *DNI* for each day and all three together.

Similarly, the influence of *DNI* on P_{mp} is shown in Figure 21. Again, the relationship is described linearly and the R^2 values 0.932, 0.9304, 0.959, 0.920 for the 03/08/2015, 13/08/2015, 19/08/2015 and all days together respectively (Table 6). Although the linear fit is considered good (range from 0.92 to 0.959), it can be seen that, on the 19/08/2015 the fit is higher than the other days, probably because the rapid changes in *AM* during the late afternoon were not measured during that day. This statement however, needs further investigation by comparing measured data from other locations and also during different seasons. Moreover, and similar to the previous case, the change in the slope of P_{mp} at around 700 W/m^2 can be observed and is expected to have been caused by the change of the limiting subcell.

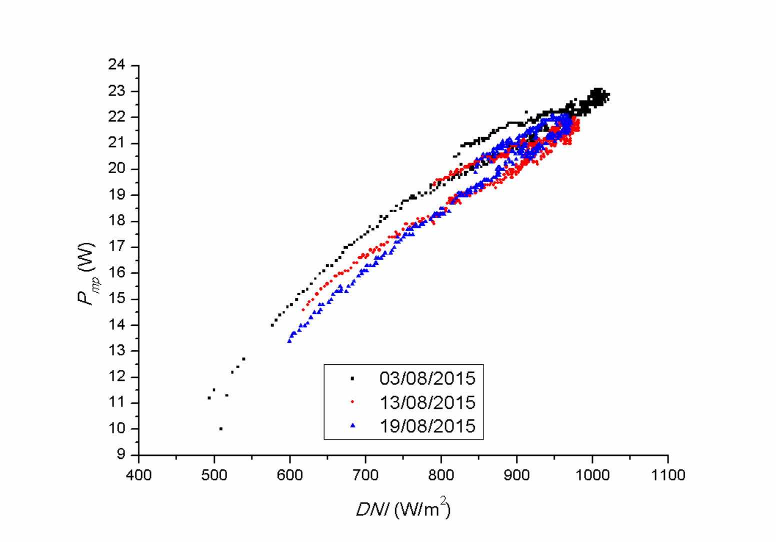

Figure 21: P_{mp} as a function of *DNI* on the 03/08/2015, 13/08/2015, 19/08/2015 in Albuquerque, NM.

Day	03/08/2015	13/08/2015	19/08/2015	All
R^2	0.932	0.9304	0.959	0.920

Table 6: R^2 values obtained by linear fit of P_{mp} Vs *DNI* for each day and all three together.

Figures 22 and 23 show the diurnal variation of electrical conversion efficiency during the selected days and the influence of *AM* on the efficiency respectively. Qualitatively, the trend is similar to the *SF* (Figure 12) with peak efficiencies during the early morning (23.2% at 07:37 am) and late afternoon hours (23.1% at 17:59 pm) on the 03/08/2015. The average efficiencies measured were 21.4%, 20.9%, 21% and the maximum 23.2%, 22.6%, 22.15% on the 03/08/2015, 13/08/2015, 19/08/2015 respectively. When the effect of *AM* on the electrical conversion efficiency is compared, it can be seen that the trend is similar to *SF* again (Figure 11), but to a lesser extent due to the other electrical parameters that affect the efficiency (e.g. voltage variations due to temperature and ligh intensity effects). It can be seen that on the 03/08/2015 the efficiency peaks when the $AM \approx 2$ but only during the morning hours where the $PW_{morning} > PW_{afternoon}$ (also discussed earlier). Again, the arrow in Figure 23 indicates the decreasing *AOD* and increasing *PW*; the combination of which, affects the performance in a positive manner (as described earlier and also in [33]).

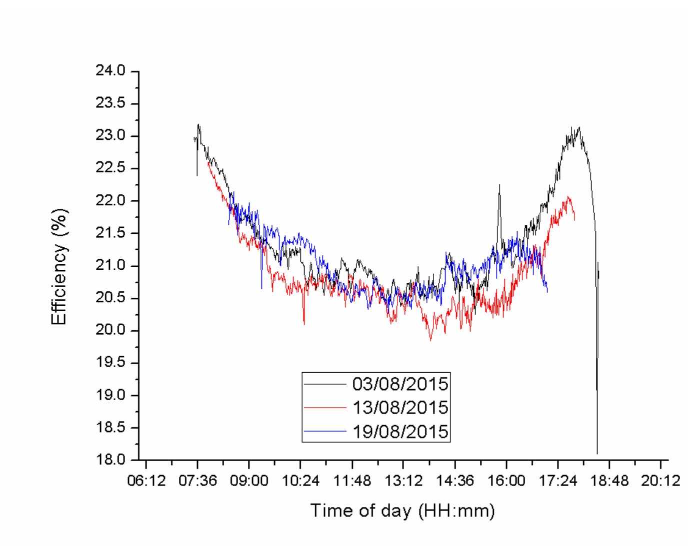

Figure 22: Diurnal variation of electrical conversion efficiency on the 03/08/2015, 13/08/2015, 19/08/2015 in Albuquerque, NM.

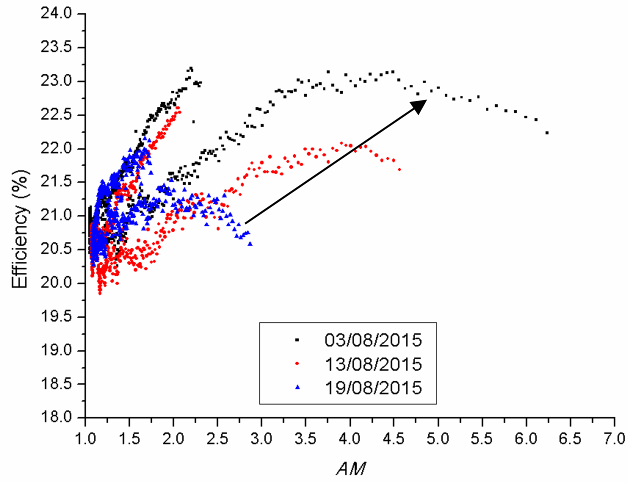

Figure 23: Influence of *AM* on electrical conversion efficiency on the 03/08/2015, 13/08/2015, 19/08/2015 in Albuquerque, NM. The arrow indicates the decreasing *AOD* and increasing *PW*.

The influence of T_{amb} on the $V_{oc}/V_{oc,ref}$ is illustrated in Figure 24; as expected the ratio is decreasing with increasing T_{amb} due to its effect on T_{cell}. The maximum value recorded was 0.945 (on the 19/08/2015 at T_{amb} = 22.1°C) while the minimum was 0.904 (on the 19/08/2015 at T_{amb} = 33.8°C), for a range of T_{amb} = 21.2°C to 34.8°C. Hence, the T_{amb} has a relatively low impact on the V_{oc} although longer datasets are required to verify this observation.

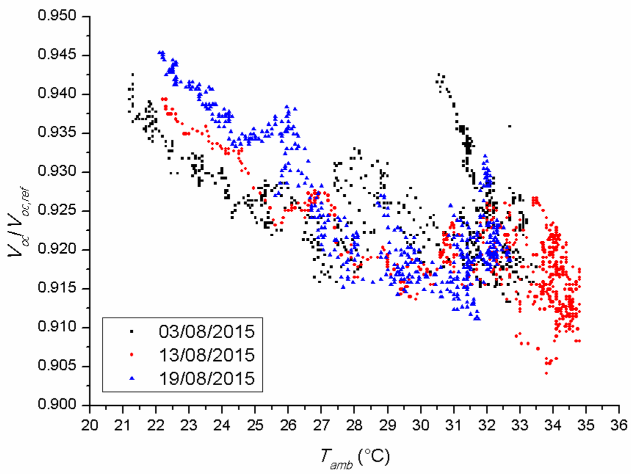

Figure 24: Ratio of $V_{oc}/V_{oc,ref}$ as a function of T_{amb} on the 03/08/2015, 13/08/2015, 19/08/2015 in Albuquerque, NM.

Similarly the I_{sc}/DNI is plotted in Figure 25; although the ratio was expected to increase with increasing T_{amb} (since the T_{diode} is increasing with T_{amb}, see Figure 26) this was not observed during the measurements. This could be caused by two effects: spectral and/or Fresnel lens thermal expansion. The spectral analysis presented earlier has shown how the performance varies during the day and the peaks observed in Figure 25 are similar to the ones of *SF*; this can be an indication that the spectral performance balances out the effect of T_{amb} on the I_{sc}/DNI. Therefore the ratio is higher when spectral gains occur and lower when losses occur. Research has also shown that the increasing temperatures can modify the optical efficiency due to the temperature dependence of the refractive index and also due to surface deformation of the Fresnel lens [38]. The effect was also noticed by García-Domingo *et al*. [39]. Further investigations are required to quantify the effect of changing Fresnel lens temperature on the optical, spectral and electrical performance of CPV systems.

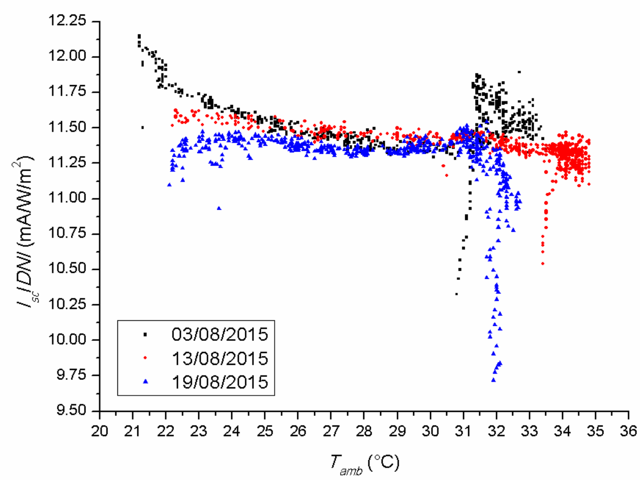

Figure 25: Ratio of I_{sc}/DNI as a function of T_{amb} on the 03/08/2015, 13/08/2015, 19/08/2015 in Albuquerque, NM.

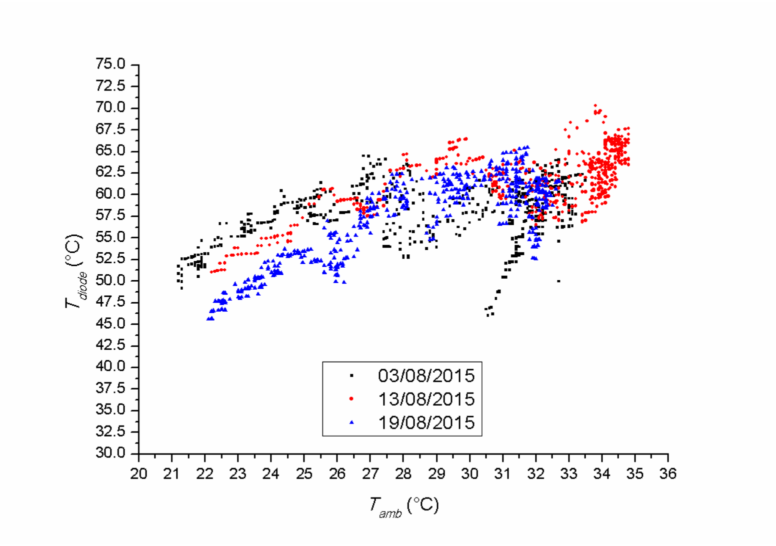

Figure 26: T_{diode} against T_{amb} on the 03/08/2015, 13/08/2015, 19/08/2015 in Albuquerque, NM.

5. Summary and conclusions

The outdoor performance of a CPV monomodule was inestigated in this study. Three relatively clear-sky days were selected in order to provide a better understanding and also to reduce the noise in the characterisation.

The influence of the solar geometry and atmospheric parameters was found to be of great importance when the spectral gains were compared between the three selected days. In particular, it was shown that on the 03/08/2015 spectral gains of up to 5% were observed due to the lower *AOD* (i.e. relatively clear atmosphere) and higher *PW* (i.e. relatively wet atmosphere). Significant differences were found in *DNI*, *SF*, *SMR* during the morning and afternoon hours, mainly because of the variation in *AOD* and *PW*.

It was observed that the electrical and spectral parameters exhibited similar trends, especially in the case of *SF* and efficiency, verifying the importance of considering the spectrum variations on CPV performance. The I_{sc} and P_{mp} exhibited a linear relationship against the *DNI*, however the spectral sensitivity of III-V 3J solar cells also plays a significant role. This was noticed when diurnal variation of the electrical conversion efficiency was plotted and also against the *AM*; the peaks were measured during the early morning and late afternoon due to the spectrum changes (also mentioned in the previous paragraph). In terms of the thermal behaviour, maximum temperatures of 70.3°C and 67.6°C were observed on the diode and heat sink respectively. The V_{oc} and I_{sc} did not exhibit a dependence on T_{amb}; this was attributed to the temperature dependence and chromatic aberrations of the Fresnel lens and that future work should try to quantify the effect based on measured data in order to extract a correction factor.

Acknowledgements

Marios Theristis acknowledges the financial support of the Royal Society of Edinburgh through the J. M. Lessells scholarship and the Center for Sustainable Energy Systems (CSE), Fraunhofer USA through the research fellowship. Eduardo F. Fernández acknowledges the Spanish Ministry of Economy and Competitiveness for the Juan de la Cierva 2015 – Incorporación fellowship and the FEDER funds under the project ENE2016-78251-R. The authors would like to thank James P. Crimmins, Larry Pratt from CFV Solar Test Laboratory and Cameron Stark, Mark Hill from CSE Fraunhofer for the technical support and useful advice. James Foresi and Mike Sumner from Suncore Photovoltaics Inc. are duly acknowledged for the useful discussions and also for generously lending the CPV monomodule used in this study.

References

[1] D. L. Talavera, J. P. Ferrer-Rodríguez, P. Pérez-Higueras, J. Terrados, and E. F. Fernández, "A worldwide assessment of levelised cost of electricity of HCPV systems," *Energy Conversion and Management*, vol. 127, pp. 679-692, 2016.

[2] P. Rodrigo, E. Fernández, F. Almonacid, and P. Pérez-Higueras, "Models for the electrical characterization of high concentration photovoltaic cells and modules: A review," *Renewable and Sustainable Energy Reviews*, vol. 26, pp. 752-760, 2013.

[3] G. S. Kinsey and K. M. Edmondson, "Spectral Response and Energy Output of Concentrator Multijunction Solar Cells," *Progress in Photovoltaics: Research and Applications*, vol. 17, pp. 279-288, Aug 2009.

[4] M. Theristis, N. Sarmah, T. K. Mallick, and T. S. O'Donovan, "Design and Numerical Analysis of Enhanced Cooling Techniques for a High Concentration Photovoltaic

(HCPV) System," in *27th European Photovoltaic Solar Energy Conference and Exhibition (EU PVSEC)*, Frankfurt, Germany, 2012, pp. 260 - 265.

[5] C. Renno, F. Petito, G. Landi, and H. C. Neitzert, "Experimental characterization of a concentrating photovoltaic system varying the light concentration," *Energy Conversion and Management,* vol. 138, pp. 119-130, 2017.

[6] E. F. Fernández, P. Pérez-Higueras, A. J. Garcia Loureiro, and P. G. Vidal, "Outdoor evaluation of concentrator photovoltaic systems modules from different manufacturers: first results and steps," *Progress in Photovoltaics: Research and Applications,* vol. 21, pp. 693-701, 2013.

[7] M. Muller, B. Marion, S. Kurtz, K. Ghosal, S. Burroughs, C. Libby, and N. Enbar, "A side-by-side comparison of CPV module and system performance," *Progress in Photovoltaics: Research and Applications*, pp. n/a-n/a, 2016.

[8] M. Theristis and T. S. O'Donovan, "Electrical-thermal analysis of III–V triple-junction solar cells under variable spectra and ambient temperatures," *Solar Energy,* vol. 118, pp. 533-546, 2015.

[9] E. F. Fernández, F. Almonacid, P. Rodrigo, and P. Pérez-Higueras, "Model for the prediction of the maximum power of a high concentrator photovoltaic module," *Solar Energy,* vol. 97, pp. 12-18, 2013.

[10] E. F. Fernández, P. Pérez-Higueras, F. Almonacid, J. A. Ruiz-Arias, P. Rodrigo, J. I. Fernandez, and I. Luque-Heredia, "Model for estimating the energy yield of a high concentrator photovoltaic system," *Energy,* 2015.

[11] M. Theristis, E. Fernández, F. Almonacid, and G. Georghiou, "Spectral Correction of CPV Modules Equipped with GaInP/GaInAs/Ge Solar Cells and Fresnel Lenses," *Applied Sciences,* vol. 7, p. 842, 2017.

[12] S. Kurtz, M. Muller, D. Jordan, K. Ghosal, B. Fisher, P. Verlinden, J. Hashimoto, and D. Riley, "Key parameters in determining energy generated by CPV modules," *Progress in Photovoltaics: Research and Applications,* vol. 23, pp. 1250-1259, 2015.

[13] J. Hashimoto, S. Kurtz, K. Sakurai, M. Muller, and K. Otani, "Field experience and performance of CPV system in different climates," in *AIP Conference Proceedings*, 2013, p. 261.

[14] M. Theristis, C. Stark, and T. S. O'Donovan, "Determination of the cooling requirements for single cell photovoltaic receivers under variable atmospheric parameters," in *Photovoltaic Specialist Conference (PVSC), 2015 IEEE 42nd*, 2015, pp. 1-5.

[15] M. Theristis, E. F. Fernández, F. Almonacid, and P. Pérez-Higueras, "Spectral Corrections Based on Air Mass, Aerosol Optical Depth, and Precipitable Water for CPV Performance Modeling," *IEEE Journal of Photovoltaics,* vol. 6, pp. 1598-1604, 2016.

[16] M. Theristis, E. F. Fernández, M. Sumner, and T. S. O'Donovan, "Multiphysics modelling and experimental validation of high concentration photovoltaic modules," *Energy Conversion and Management,* vol. 139, pp. 122-134, 2017.

[17] E. F. Fernández, F. Almonacid, A. Soria-Moya, and J. Terrados, "Experimental analysis of the spectral factor for quantifying the spectral influence on concentrator photovoltaic systems under real operating conditions," *Energy,* vol. 90, pp. 1878-1886, 2015.

[18] M. Theristis, E. F. Fernández, G. E. Georghiou, and T. S. O'Donovan, "Performance of a concentrating photovoltaic monomodule under real operating conditions: Part II – Power rating," *Energy Conversion and Management (under review),* 2017.

[19] "Standard IEC 62670-3, "Concentrator Photovoltaic (CPV) - Performance Testing Part 3: Performance Measurements and Power Rating," 2017, Geneva, Switzerland.," ed.

[20] "ASTM G173-03(2012), Standard Tables for Reference Solar Spectral Irradiances: Direct Normal and Hemispherical on 37° Tilted Surface, ASTM International, West Conshohocken, PA, 2012, www.astm.org," ed.
[21] C. Domínguez, I. Antón, G. Sala, and S. Askins, "Current-matching estimation for multijunction cells within a CPV module by means of component cells," *Progress in Photovoltaics: Research and Applications,* vol. 21, pp. 1478-1488, 2013.
[22] R. Núñez, C. Domínguez, S. Askins, M. Victoria, R. Herrero, I. Antón, and G. Sala, "Determination of spectral variations by means of component cells useful for CPV rating and design," *Progress in Photovoltaics: Research and Applications,* vol. 24, pp. 663-679, 2016.
[23] P. M. Rodrigo, E. F. Fernández, F. M. Almonacid, and P. J. Pérez-Higueras, "Quantification of the spectral coupling of atmosphere and photovoltaic system performance: Indexes, methods and impact on energy harvesting," *Solar Energy Materials and Solar Cells,* vol. 163, pp. 73-90, 2017.
[24] R. Núñez, C. Jin, M. Victoria, C. Domínguez, S. Askins, R. Herrero, I. Antón, and G. Sala, "Spectral study and classification of worldwide locations considering several multijunction solar cell technologies," *Progress in Photovoltaics: Research and Applications*, pp. n/a-n/a, 2016.
[25] "Standard IEC 60904-7, "Photovoltaic devices - Part 7: Computation of the spectral mismatch correction for measurements of photovoltaic devices," 2008.," ed.
[26] G. Nofuentes, B. García-Domingo, J. V. Muñoz, and F. Chenlo, "Analysis of the dependence of the spectral factor of some PV technologies on the solar spectrum distribution," *Applied Energy,* vol. 113, pp. 302-309, 2014.
[27] E. F. Fernández, F. Almonacid, J. A. Ruiz-Arias, and A. Soria-Moya, "Analysis of the spectral variations on the performance of high concentrator photovoltaic modules operating under different real climate conditions," *Solar Energy Materials and Solar Cells,* vol. 127, pp. 179-187, 2014.
[28] G. Peharz, G. Siefer, and A. W. Bett, "A simple method for quantifying spectral impacts on multi-junction solar cells," *Solar Energy,* vol. 83, pp. 1588-1598, 2009.
[29] J. Jaus, T. Mißbach, S. Philipps, G. Siefer, and A. Bett, "Spectral measurements using component cells: Examinations on measurement precision," in *26th European Photovoltaic Solar Energy Conference and Exhibition (EU PVSEC),* Hamburg, Germany, 2011, pp. 1-6.
[30] R. W. Higgins, Y. Yao, and X. L. Wang, "Influence of the North American Monsoon System on the U.S. Summer Precipitation Regime," *Journal of Climate,* vol. 10, pp. 2600-2622, 1997/10/01 1997.
[31] C. A. Gueymard, D. Myers, and K. Emery, "Proposed reference irradiance spectra for solar energy systems testing," *Solar Energy*, vol. 73, pp. 443-467, 2002.
[32] F. Kasten and A. T. Young, "Revised optical air mass tables and approximation formula," *Applied Optics,* vol. 28, pp. 4735-4738, 1989/11/15 1989.
[33] M. Theristis, E. F. Fernández, C. Stark, and T. S. O'Donovan, "A theoretical analysis of the impact of atmospheric parameters on the spectral, electrical and thermal performance of a concentrating III–V triple-junction solar cell," *Energy Conversion and Management,* vol. 117, pp. 218-227, 2016.
[34] M. Muller, B. Marion, S. Kurtz, J. Rodriguez, A. W. Bett, R. D. McConnell, G. Sala, and F. Dimroth, "An investigation into spectral parameters as they impact CPV module performance," in *AIP Conference Proceedings*, 2010, p. 307.
[35] M. Theristis, E. F. Fernández, J. P. Ferrer-Rodríguez, C. Stark, and T. S. O'Donovan, "Energy yield assessment of a high concentration photovoltaic receiver based on

simulated spectra from typical meteorological year datasets," in *AIP Conference Proceedings*, 2016, p. 090009.

[36] W. E. McMahon, K. E. Emery, D. J. Friedman, L. Ottoson, M. S. Young, J. S. Ward, C. M. Kramer, A. Duda, and S. Kurtz, "Fill factor as a probe of current-matching for GaInP2/GaAs tandem cells in a concentrator system during outdoor operation," *Progress in Photovoltaics*, vol. 16, pp. 213-224, May 2008.

[37] E. F. Fernández, G. Siefer, F. Almonacid, A. J. G. Loureiro, and P. Perez-Higueras, "A two subcell equivalent solar cell model for III-V triple junction solar cells under spectrum and temperature variations," *Solar Energy*, vol. 92, pp. 221-229, Jun 2013.

[38] T. Hornung, M. Steiner, and P. Nitz, "Estimation of the influence of Fresnel lens temperature on energy generation of a concentrator photovoltaic system," *Solar Energy Materials and Solar Cells*, vol. 99, pp. 333-338, 2012.

[39] B. García-Domingo, J. Aguilera, J. de la Casa, and M. Fuentes, "Modelling the influence of atmospheric conditions on the outdoor real performance of a CPV (Concentrated Photovoltaic) module," *Energy*, vol. 70, pp. 239-250, 2014.

Nomenclature

AM	air mass
AOD	aerosol optical depth
DNI	direct normal irradiance, W/m^2
FF	fill factor
GNI	global normal irradiance W/m^2
I	current, A
J	current density, A/m^2
P	power output, W
PW	precipitable water, cm
SF	spectral factor
SMR	spectral matching ratio
SR	spectral response
T	temperature, °C
V	voltage, V
WS	wind speed, m/s
z	zenith angle, °

Greek letters

η	efficiency
λ	wavelength, nm

Subscripts

amb – ambient

HS – heat sink

mp – maximum power

oc – open-circuit

opt – optical

ref - reference

sc – short-circuit

Abbreviations

BPI – Black Photon Instruments

CPV – Concentrating photovoltaic

DBC - Direct Bonded Copper

IEC – International Electrotechnical Commission

MJ - Multijunction

PV - Photovoltaic

SoG – Silicon-on-Glass

TC – Thermocouple

3J - Triple-junction